

# Extended Spectral Analysis of Multiple Beam Interferometry: A Technique To Study Metallic Films in the Surface Forces Apparatus

John M. Levins and T. Kyle Vanderlick\*

Department of Chemical Engineering, University of Pennsylvania,  
Philadelphia, Pennsylvania 19104-6393

Received February 24, 1994. In Final Form: May 4, 1994<sup>®</sup>

We introduce a new technique, extended spectral analysis of multiple beam interferometry (ESA-MBI), which significantly expands the variety of surfaces that can be investigated in the surface forces apparatus (SFA). The underlying principle of the technique is to capture the intensity versus wavelength profile of light transmitted through the surfaces; the distance between them is then determined by matching the measured spectra with that predicted from the theory of wave propagation through a stratified medium. ESA-MBI requires two key ingredients: (1) a camera system capable of measuring the intensity versus wavelength spectra and (2) the implementation of theory to predict it. We describe these two ingredients and show how ESA-MBI can be used in conjunction with the SFA to investigate the interactions between two opposed surfaces where one, or both of the surfaces is metallic. Finally, we describe a procedure wherein ESA-MBI is employed to measure the refractive indices of thin metal films, and we report our results for thermally evaporated silver and gold. This procedure is necessary to maximize the accuracy of surface separation measurements.

## Introduction

Multiple beam interferometry (MBI), a technique put on firm ground by Tolansky,<sup>1</sup> is often relied upon to measure accurately the thickness or refractive index of thin films. The technique requires the construction of an "interference filter" composed of two reflective layers separated by one or more layers of dielectric media. Only certain wavelengths of light incident on the filter pass through with appreciable intensity. The allowed wavelengths can be tuned continuously by varying the distance between the reflective layers. MBI has been used in this manner in conjunction with the well-known surface forces apparatus (SFA) to measure changes in the thickness of a film confined between two opposed surfaces.

Although a wide variety of colloidal and adhesive interactions have been investigated with the SFA,<sup>2-4</sup> these applications have utilized MBI in a limited capacity. In particular, silver has been exclusively used as the reflective film, generating filters which transmit extremely sharp bands of light. These bands were named "fringes of equal chromatic order" (FECO) by Tolansky.<sup>1</sup> Moreover, the type of filter used in the SFA has predominantly been of the form silver/mica/medium/mica/silver. Upon dispersion, the FECO generated from these silver-based filters are just narrow enough and just bright enough that very small shifts—corresponding to angstrom level changes in the medium thickness—can be measured by eye. Furthermore, the measured shifts are readily interpreted using simple analytical expressions derived for filters bounded by perfectly reflective layers.<sup>5,6</sup> Clearly, this "conventional application" of MBI inherently restricts the variety of surfaces that can be examined in the SFA.

In this paper we introduce a new technique, called extended spectral analysis of multiple beam interferometry (ESA-MBI) which no longer relies on the efficiency of the silver-based filter. The technique permits other types of metals, and thus surfaces, to be studied in the SFA without sacrificing the precision of the distance measurements. This is basically accomplished by measuring, as a function of wavelength, the intensity of light transmitted through a filter. The unknown thickness, which is needed to predict the transmitted spectra, is then determined by matching the calculated spectra with that measured. Unlike conventional MBI, which is not concerned with the details of the transmitted spectra, our technique can be used to extract additional information contained in the intensity versus wavelength profiles, such as surface roughness.<sup>7</sup>

Our technique is based on two key ingredients. The first is the hardware necessary to capture the entire spectra transmitted through less efficient filters. The second is the implementation of the theory of electromagnetic wave propagation in a stratified medium to predict the spectra and match it against experiment. In this paper, we elaborate on these ingredients and show how ESA-MBI can be applied to measure changes in film thicknesses inside interference filters composed of metals other than silver. Finally, we describe and implement a procedure where ESA-MBI is employed to measure the refractive indices of metal films. We report our results for thermally evaporated silver and gold.

## Description of ESA-MBI

We divide our description of ESA-MBI into two sections: (A) The equipment necessary to capture the transmitted spectra and (B) the theory used to predict it.

**A. Equipment.** ESA-MBI requires an instrument that can measure quantitatively and accurately the intensity versus wavelength of light transmitted through an interference filter. Since the transmitted light is weak, the instrument must be capable of measuring the intensity of very dim images. We have chosen to use a liquid-cooled

\* To whom correspondence should be addressed.

<sup>®</sup> Abstract published in *Advance ACS Abstracts*, July 1, 1994.

(1) Tolansky, S. *Multiple-Beam Interferometry of Surfaces and Films*; Oxford University Press: London, 1948.

(2) Israelachvili, J. N.; McGuigan, P. M. *Science* **1988**, *241*, 795.

(3) Israelachvili, J. N. *J. Vac. Sci. Technol. A* **1992**, *10*, 2961.

(4) Israelachvili, J. N. *Intermolecular and Surface Forces*; Academic Press: London, 1985.

(5) Israelachvili, J. N. *J. Colloid Interface Sci.* **1973**, *44*, 259.

(6) Horn, R. G.; Smith, D. T. *Appl. Opt.* **1991**, *30*, 59.

(7) Levins J. M.; Vanderlick, T. K. *J. Colloid Interface Sci.* **1993**, *158*, 223.

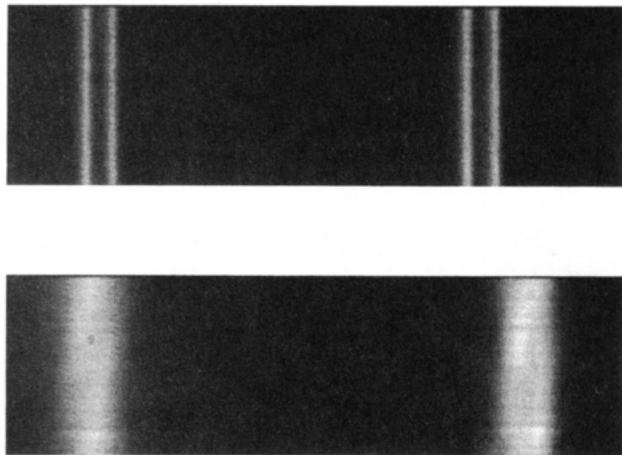


**Figure 1.** Images incident on the CCD chip of the camera for two types of filters. Each filter is composed of a single mica sheet, approximately  $3.5 \mu\text{m}$  thick, coated on both sides with a metal film. The top image is from a silver-coated filter ( $512 \text{ \AA}$  on one side,  $400 \text{ \AA}$  on the other) and the bottom image is from a gold-coated filter ( $525 \text{ \AA}$  on both sides). The spot on the left-most FECO for the gold-coated filter is due to a piece of dust on the mirror used to reflect the image to the CCD.

slow-scan charge-coupled-device (CCD) imaging system (Photometrics Series 200). The hub of the system is the CCD detector, a chip comprised of an array of square pixels ( $25 \mu\text{m}$  on a side), which can be exposed to the image for time intervals of 0.1 to 1000 s. Light incident on each pixel generates a charge which is proportional to the intensity and the exposure time. The CCD readout is given in arbitrary units, which we refer to as "counts."

The camera is mounted on the exit port of a spectrometer, which disperses the light that passes through the interference filter. (The CCD detector is focused using the method described by Deitrick.<sup>8</sup>) The images of light transmitted through two filters are shown in Figure 1, as recorded by the camera (the measured counts for each pixel have been converted to a gray scale and displayed on a computer monitor). Both filters consist of a single mica sheet, coated on both sides with a metallic film. Silver films are used in the first filter, gold in the second. (Preparation procedures are described in Appendix I.) Each picture consists of 100 rows  $\times$  570 columns of pixels. Notice that the intensity peaks are sharp for the silver filter (they appear as doublets because mica is birefringent); however, for the gold filter, they are blurry and broad.

The measured intensity versus pixel profiles corresponding to the pictures in Figure 1 are shown in Figure 2. The exposure time is 3 s for the silver filter and 10 s for the gold filter. Note that the signal-to-noise ratio is better for the longer exposure time. For this reason, we have used a 10-s exposure time for all of the results that are reported in this paper. The signal-to-noise ratio can also be improved by averaging the signal across several rows. The profiles in Figure 2, and all of the results reported here, are the average of signal measured along the center seven rows.

To compare the camera's image with theory, which will be described in the next section, it is necessary to convert the intensity versus *pixel* profile to an intensity versus *wavelength* profile. This is done by exposing the camera to dispersed mercury light composed of spectral lines of known wavelength. The positions of the mercury lines on the detector are thus used to calibrate the dispersion of

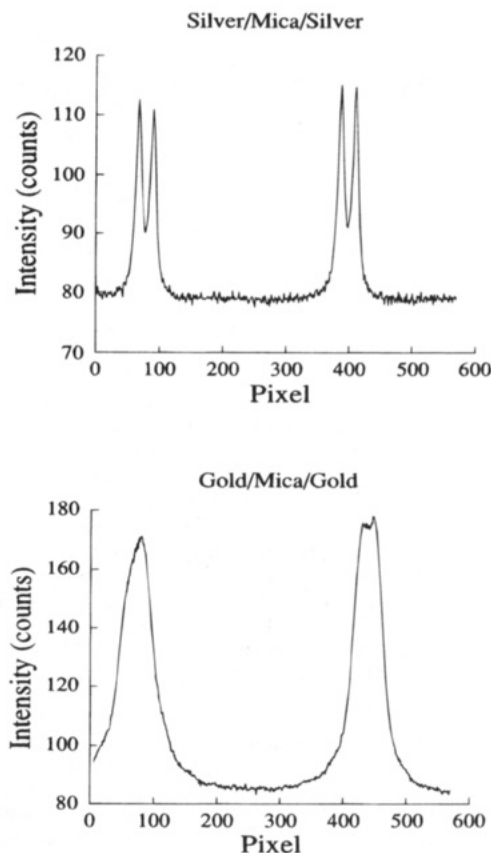


**Figure 2.** Measured intensity versus pixel profiles of the light transmitted through the two filters shown in Figure 1.

the spectrometer in terms of  $\text{\AA}/\text{pixel}$ . For our spectrometer, the dispersion is  $0.7582 \text{ \AA}/\text{pixel}$ .

The detector is housed in a liquid-cooled camera head ( $-45 \text{ }^\circ\text{C}$ ) which greatly reduces, but does not eliminate, charge accumulation arising from background noise. This background can be measured by exposing the CCD detector to darkness after each intensity versus wavelength profile is captured. We have found that the background signal is uniform across the CCD chip and shows no dependence on exposure time from 3 to 10 s. The typical average background signal is 80 counts, with an average standard deviation of 1 count. Over all of our experiments the average background signal has been between 78 and 83 counts. In all of the intensity versus wavelength profiles that will be shown in this paper, we have subtracted off the background signal.

**B. Theory.** The intensity versus wavelength of light transmitted through an interference filter can be calculated using the method described in Born and Wolf,<sup>9</sup> referred to as the "multilayer matrix method" by Clarkson.<sup>10</sup> Consider white light incident normal to the layers of an interference filter. Each layer has a thickness  $z_j$  and a refractive index  $\mu_j$  (for metals,  $\mu_j$  is complex). Each layer can be described by a characteristic matrix  $\bar{M}_j$

$$\bar{M}_j = \begin{pmatrix} \cos q_j & -(i/\mu_j) \sin q_j \\ -i\mu_j \sin q_j & \cos q_j \end{pmatrix}$$

where

$$q_j = \frac{2\pi\mu_j z_j}{\lambda}$$

Here,  $\lambda$  is the wavelength of light in a vacuum. The

(8) Deitrick, G. L. PhD. Thesis, University of Minnesota, 1990; Chapter 4.2.

(9) Born, M.; Wolf, E. *Principles of Optics*, 6th ed.; Pergamon Press: Oxford, 1980.

(10) Clarkson, M. T. *J. Phys. D* **1989**, *22*, 475.

characteristic matrix of a multilayer consisting of a succession of layers is simply

$$\bar{M} = \prod_j \bar{M}_j$$

The transmission coefficient,  $t$ , of the multilayer is given by

$$t(\lambda) = \frac{2\mu^i}{(m_{11} + m_{12}\mu^e)\mu^i + m_{21} + m_{22}\mu^e}$$

where  $m_{ij}$  values are the elements of  $\bar{M}$ , and  $\mu^i$  and  $\mu^e$  are the refractive indices of the semi-infinite medium that surrounds the filter, on the incident and emergent sides, respectively. The transmissivity,  $\mathcal{T}$ , is defined as the ratio  $I(\lambda)/I_0(\lambda)$ , where  $I(\lambda)$  and  $I_0(\lambda)$  are the intensities of light transmitted through, and incident to, the filter, respectively.  $\mathcal{T}(\lambda)$  can be calculated from  $t(\lambda)$  using the expression

$$\mathcal{T}(\lambda) = \frac{\mu_e}{\mu_i} |t(\lambda)|^2$$

So as to keep our notation less cluttered, we will no longer carry the wavelength dependence of  $I$ ,  $I_0$ , and  $\mathcal{T}$ ; however, it is understood that all three variables are functions of  $\lambda$ .

Thus, provided all the  $z_j$  and  $\mu_j$  are known, the transmissivity versus wavelength profile,  $\mathcal{T}$ , can be predicted. Furthermore, if any single  $z_j$  or  $\mu_j$  is unknown, then it can be determined by finding that value which gives the best match between the predicted spectra and that measured. This is the principle by which ESA-MBI works.

Now that we have described the formal theory, there are three important details that must be accounted for to properly compare experimental data with theory. First, in all of the filters used herein at least one of the layers is mica, a birefringent material with two indices of refraction, typically denoted  $\mu^\beta$  and  $\mu^\gamma$ . (Values of  $\mu^\beta$  and  $\mu^\gamma$  are given in Appendix II.) Light transmitted through the mica is split into two parts. One part experiences the  $\beta$  component of the refractive index, the other part the  $\gamma$  component. To account for this, we calculate  $\mathcal{T}$  for each component, then average the two spectra to yield the net  $\mathcal{T}$ . The superposition of the two individual spectra—one slightly shifted from the other—results in a broadening of the peaks in the net  $\mathcal{T}$ , in some cases leading to an observable splitting into doublets (see Figures 1 and 2).

Second, we must account for the broadening of  $\mathcal{T}$  that is caused simply by the finite width of light admitted into the spectrometer. This phenomenon, which we have described in detail in a previous publication (termed the "slit effect"),<sup>7</sup> is governed by three parameters: the width of the spectrometer slit, the dispersion of the spectrometer, and the magnification of the optical train. For our particular setup, these parameters are as follows: slit width of 100  $\mu\text{m}$ , dispersion of 0.0327  $\text{\AA}/\mu\text{m}$ , and magnification of 18.2.

Third, the measured intensity transmitted through a filter,  $I$ , must be converted to transmissivity,  $\mathcal{T}$ . This is accomplished by dividing  $I$  by the incident intensity,  $I_0$ , which is the intensity of light measured in the absence of the filter. We have measured  $I_0$  and found that for our particular white light source, the intensity is not constant with wavelength over the visible spectrum. The intensity increases linearly with wavelength from 5410 to 5500  $\text{\AA}$ , reaching a plateau value,  $\bar{I}_0$ , that holds until 5775  $\text{\AA}$ , where it again increases linearly until 5840  $\text{\AA}$ . At 5410  $\text{\AA}$ ,  $I_0$  is 80% of  $\bar{I}_0$ , and at 5840  $\text{\AA}$  it is 104% of  $\bar{I}_0$ . This dependence on wavelength is consistent for all of the measurements

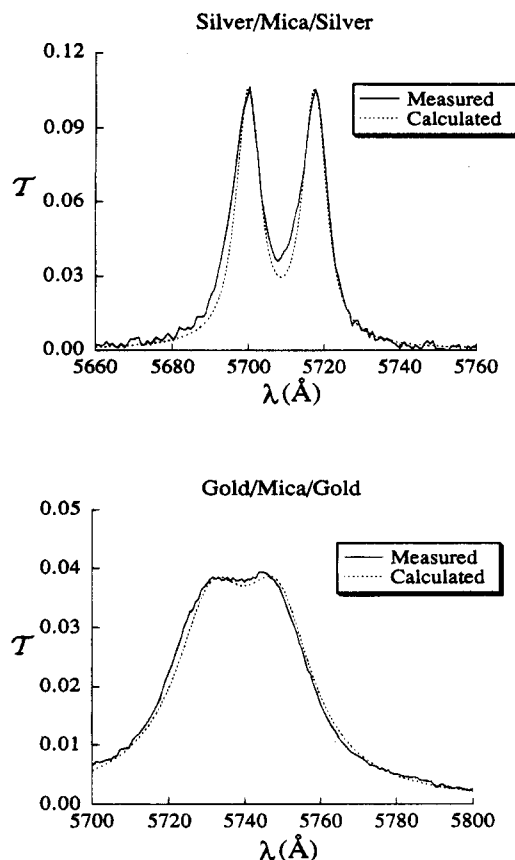


Figure 3. Measured and calculated  $\mathcal{T}$  for both filters shown in Figure 1.

we have made. However, we have also found that the magnitude of  $I_0$  is highly sensitive to minor changes in the exact positions of the several lenses and quartz disks used in the experiments (see Appendix I). For example, over seven different measurements, each for a slightly different lens setup, we found that  $\bar{I}_0$  varied from 1650 to 2300 counts. Thus, even the slight perturbation in the optical setup caused by removing the filter is enough to significantly change the incident intensity.

Since we are not able to obtain an accurate measure of  $I_0$ , we use the following protocol to convert  $I$  to  $\mathcal{T}$ , which properly accounts for the wavelength dependence of  $I_0$ . Within the wavelength range encompassed by the plateau, we find the maximum measured intensity,  $I_{\text{max}}$ , and the maximum calculated transmissivity,  $\mathcal{T}_{\text{max}}$ . Then, the plateau intensity is determined by  $\bar{I}_0 = I_{\text{max}}/\mathcal{T}_{\text{max}}$ . The incident intensity at all wavelengths is then calculated relative to  $\bar{I}_0$ , as based on the wavelength dependence of  $I_0$  stated above. For all of the results reported in this paper, we report the value of  $\bar{I}_0$ . It is not disconcerting that  $\bar{I}_0$  must be adjusted as opposed to measured, since it is merely a scaling factor and does not affect the two most important features of the transmitted spectra: the locations and shape of the peaks.

Two examples of the comparison between theoretical prediction and experimental measurement of  $\mathcal{T}$  are shown in Figure 3. The data shown correspond to the right-most peaks displayed in Figure 1. The measured profile matches the predicted profile extremely well for both filters, demonstrating how well the two components of the ESA-MBI technique complement each other and showing that theory can be relied upon to accurately predict  $\mathcal{T}$ .

In practice all the layers of a real filter are not smooth, as we have assumed so far. It is possible, however, to appeal to the theory to describe the impact of roughness

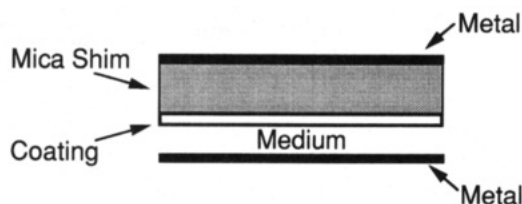


**Figure 4.** A schematic of a filter that can be used with ESA-MBI in the SFA to study the interactions between two surfaces where one, or both, of the surfaces is metallic.

on  $\mathcal{F}$ . We showed previously how it is possible to calculate  $\mathcal{F}$  for filters where one or more of the layers is rough.<sup>7</sup> We note here that one of our findings was that only roughness in the interior of the filter affects  $\mathcal{F}$ ; roughness on the outside can be ignored. The mica sheets used in the filters shown in Figures 1–3 are prepared so their surfaces are molecularly smooth. Thus, we are able to ignore roughness, as we did in the calculations of Figure 3.

The remainder of this paper is divided as follows. In the next section we describe how ESA-MBI can be used in conjunction with the SFA to investigate surfaces where one or both are metallic. Finally, we describe a simple yet important application of ESA-MBI to determine accurately the refractive indices of metal films.

### Implementation of ESA-MBI in Conjunction with the SFA

We are interested in using the SFA to study the forces acting between surfaces where one, or both, of the surfaces is metal. Shown in Figure 4 is a schematic of a robust filter suitable for such experiments. This filter is designed to measure the forces acting between the lower metal film and the coating on mica. The separation between these surfaces is equal to the thickness of the medium trapped between them, which is measured using ESA-MBI. The coating on the mica surface could be a dielectric material (such as polymers,<sup>11–13</sup> Langmuir-Blodgett films,<sup>14</sup> and surfactant monolayers<sup>15</sup>) or a thin metal. The mica sheet itself is included in the filter to act as a shim between the outermost reflective metals, to ensure that peaks in  $\mathcal{F}$  within the visible spectrum occur. (The shim must be greater than approximately  $1 \mu\text{m}$ .) Muscovite mica is an ideal material for use as a shim because it can be cleaved into thin sheets with molecularly smooth surfaces. We, along with others,<sup>16–18</sup> have used this filter to study the forces acting between a bare mica surface and the surface of a silver film; in those experiments, conventional MBI was used.

By use of the technique of ESA-MBI, the restriction to using silver films is abolished. Any type of reflective film can be used in the filter, the only requirement being that enough signal must be transmitted to be detected by the camera. ESA-MBI thus opens up the opportunity to study a wide variety of metal surfaces in the SFA, representing a significant advance in the field of surface forces.

Given the enormous variety of filters that can be used with ESA-MBI, we want to point out that theory can serve as an invaluable design tool to predict  $\mathcal{F}$  for any type of filter prior to constructing it in the laboratory. For example, the influence of variables such as metal or mica thickness on the sharpness and intensity of transmitted peaks can be assessed before performing experiments.

One of the more novel applications of the SFA that is now possible is the study of the forces acting between two metal surfaces. The appropriate filter for these experiments consists of not two, but three reflective layers. We have used theory to verify that angstrom-level changes in the separation between the two metal surfaces (composed of either silver or gold) will induce a measurable shift in  $\mathcal{F}$ .

To date, only one study has been done where the SFA was used to measure the interactions between two metal surfaces;<sup>19</sup> in particular, platinum films were studied. Conventional MBI was employed, however, and thus extremely thin metal films (4 nm) were used so that the transmitted spectra could be observed by eye. ESA-MBI is not hampered by such requirements since the camera exposure can be increased to capture extremely dim images.

It is conceivable that one might not know some of the thicknesses and/or refractive indices of the layers composing a desired filter. Recall that the general operating principle of ESA-MBI is to determine one unknown (a thickness or refractive index) within a filter by finding that value which best matches theory to experiment. The accuracy and precision of this determination are dependent on how well the thicknesses and refractive indices of the other filter components are known. In practice, the mica shim thickness,  $z_m$ , is not known since a new sheet must be cleaved for each experiment. Although the refractive indices of most metals are available, they may not be accurate since it has been shown that the refractive indices of thin metal films can vary significantly depending upon the method of preparation.<sup>20,21</sup> In the last section of this paper, we show how ESA-MBI can be used to determine the unknowns just described.

### An Application of ESA-MBI: Measurement of Mica Thickness and Metal Refractive Index

We now describe an experiment that can be performed to accurately determine unknowns generally encountered in practice, in particular, the mica thickness,  $z_m$ , and metal refractive index,  $\mu_{\text{metal}}$  (which is complex where  $\mu_{\text{metal}} = n + ik$ ). The experimental procedure is general and can be applied to filters composed of any metal. We report here our results for refractive indices of thermally evaporated silver and gold films.

The experiment requires the construction of two types of filters. Its success relies on the fact that mica can be cleaved into large sheets of uniform thickness (several  $\text{cm}^2$ ), thus allowing many small squares (approximately  $1 \text{cm}^2$ ) of identical thickness to be cut out of them. Filter 1 is a mica sheet coated on both sides with metal. Filter 2 is composed of two mica sheets, each coated only on one side with the metal, with the bare mica surfaces in contact. The SFA is used to bring the mica surfaces into contact (described in Appendix I). In both cases, all three mica sheets have the same thickness  $z_m$ . The basic procedure is to measure  $\mathcal{F}$  for both filters and compare with

(11) Proust, J.-E.; Perez, E.; Segui, Y.; Montalan, D. *J. Colloid Interface Sci.* **1988**, *126*, 629.

(12) Luckham, P. P.; Klein, J. *Macromolecules* **1985**, *18*, 721.

(13) Hadziioannou, G.; Patel, S.; Granick, S.; Tirrell, M. *J. Am. Chem. Soc.* **1986**, *108*, 2869.

(14) Claesson, P. M.; Christenson, H. K. *J. Phys. Chem.* **1988**, *92*, 1650.

(15) Chen, Y. L.; Helm, C. A.; Israelachvili, J. N. *J. Phys. Chem.* **1991**, *95*, 10736–10747.

(16) Levins, J. M.; Vanderlick, T. K. *J. Phys. Chem.* **1992**, *96*, 10405.

(17) Coakley, C. J.; Tabor, D. *J. Phys. D* **1978**, *11*, L77.

(18) Parker, J. L.; Christenson, H. K. *J. Chem. Phys.* **1988**, *88*, 8013.

(19) Smith, C. P.; Maeda, M.; Atanasoska, L.; White, H. S.; McClure, D. *J. Phys. Chem.* **1988**, *92*, 199.

(20) Heavens, O. S. *Optical Properties of Thin Solid Films*; Dover Publications Inc.: New York, 1991.

(21) Abeles, F. In *Physics of Thin Films*; Academic Press: New York, 1971; Vol. 6.

theoretical predictions for various values of the unknowns  $z_m$ ,  $n$ , and  $k$ . The values of the unknowns are determined so that theory and experiment match the best.

The implementation of this procedure must account for two practical details associated with the refractive indices of metal and mica, respectively. We next describe these details and then put forth our algorithm for determining the sought unknowns,  $z_m$ ,  $n$ , and  $k$ .

First, the refractive index of metals may depend strongly on wavelength. We therefore have simplified our analysis for gold and silver by assuming that our values of  $n$  and  $k$  are very close to those measured by Johnson and Christy,<sup>22</sup> who have made the most accurate measurements to date. Thus

$$k(\lambda) = k(\lambda)_{JC} + \Delta k$$

$$n(\lambda) = n(\lambda)_{JC} + \Delta n$$

where  $n(\lambda)_{JC}$  and  $k(\lambda)_{JC}$  are the values of Johnson and Christy (detailed in Appendix II). The unknowns to be determined are therefore  $\Delta k$  and  $\Delta n$ .

Second, we consider the two mica sheets in filter 2 to have an effective birefringence which will depend on the relative crystallographic orientation of the two mica sheets. When the two sheets are oriented as in uncleaved mica, the birefringence is maximum and equal to that for a single sheet (as given in Appendix II). The degree of birefringence decreases with increasing mismatch between the mica, until there is no birefringence for perfectly mismatched sheets. Since we do not know the exact orientation of the two sheets in filter 2, we cannot predict the shape of  $\mathcal{T}$ , the peaks of which are broadened due to birefringence. In predicting the spectra for filter 2 we therefore assume the degree of birefringence is zero and comparisons between theory and experiment are based on matching solely the locations of the centers of the peaks in  $\mathcal{T}$ .

Our algorithm for determining  $z_m$ ,  $\Delta k$ , and  $\Delta n$  consists of two steps. The first is to obtain the best match between measurement and theory of the locations, in wavelength, of the peaks in  $\mathcal{T}$  for both filters 1 and 2. This is accomplished by varying only  $z_m$  and  $\Delta k$ , since changes in  $\Delta n$  do not affect peak locations. Once  $z_m$  and  $\Delta k$  are determined, the second step is to determine  $\Delta n$  so the shapes of the measured peaks best match those predicted. This step is carried out only for filter 1, since we know its birefringence. Although it is not necessary to do so, if desired the effective refractive indices of the mica in filter 2 can be determined by finding those values so the shapes of the calculated peaks best match those measured.

Measured  $\mathcal{T}$  for filters 1 and 2 with gold films as the reflective layers are shown in Figure 5, along with the best match calculated  $\mathcal{T}$ . Here, we found  $z_m = 33\,606$  Å,  $\Delta n = 0.00$ , and  $\Delta k = 0.35$ . Also, the effective refractive indices for the mica in filter 2 were found to be  $\mu_0^\beta = 1.5807$  and  $\mu_0^\gamma = 1.5833$ . Clearly, the match between experiment and theory is very good. We have repeated the same experiment for silver films and have found  $\Delta n = 0.05$  and  $\Delta k = 0.15$ . Even though the corrections to Johnson and Christy's measurements are small, they have a significant impact on the agreement between the predicted and measured spectra.

We expect the values of  $\Delta n$  and  $\Delta k$  to be the same for all experiments where the method of preparation of the metal films is the same. To check this, we prepared three different filters, each consisting of a mica sheet of identical thickness. The first was coated on both sides with silver, the second on both sides with gold, and the third on one

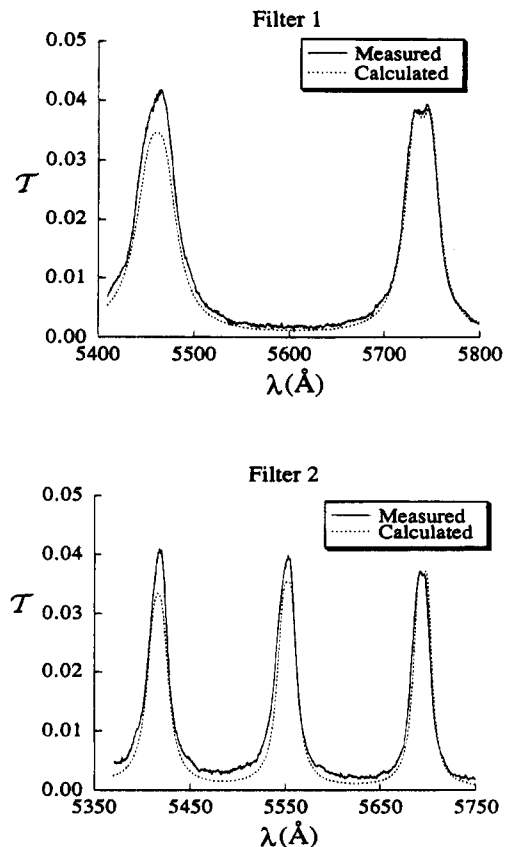


**Figure 5.** Measured and calculated  $\mathcal{T}$  for filter 1 and filter 2. Gold is used as the reflective film in both. The following parameters were used in the calculations:  $\Delta k = 0.35$ ,  $\Delta n = 0.00$ ,  $z_m = 33\,606$  Å, gold thickness 525 Å. For filter 1,  $I_0 = 2466$  and for filter 2,  $I_0 = 2892$ .

side with silver and the other side with gold.  $\mathcal{T}$  was measured for each filter and  $z_m$  was determined, given the values of  $\Delta n$  and  $\Delta k$  determined above. Shown in Figure 6 are the measured and predicted  $\mathcal{T}$  for all three filters. The  $z_m$  values are noted in the figure caption and are all very close (within 10 Å). Note also that the predicted and measured shapes of  $\mathcal{T}$  match very well, supporting our assumption that the metal refractive indices are constant from one experiment to another. This means that metal refractive indices only need to be determined once for a given preparation procedure.

The experiments that we have just described can be used to determine other unknown thicknesses as well. For instance, the thickness of the mica coating shown in Figure 4 may also not be known. Once  $z_m$  and  $\mu_{\text{metal}}$  have been determined, all that is required is an additional experiment wherein only one thickness or refractive index is unknown.  $\mathcal{T}$  can be measured and the unknown determined.

**Acknowledgment.** We gratefully acknowledge the support for this work provided by the David and Lucile Packard Foundation, the National Science Foundation Presidential Young Investigator Program (Grant CTS-89-57051), the National Science Foundation MRL Program (Grant DMR88-1998), and a Henkel Corporation Colloid and Surface Science Fellowship awarded to J.M.L. We also wish to acknowledge Jeremy Blumenfeld, who wrote the data acquisition software for the CCD camera.

#### Appendix I: Preparation of Interference Filters

The method of preparing interference filters is as follows. Thin sheets of ruby muscovite mica were cleaved as

(22) Johnson, P. B.; Christy, R. W. *Phys. Rev. B* **1972**, *6*, 4370.

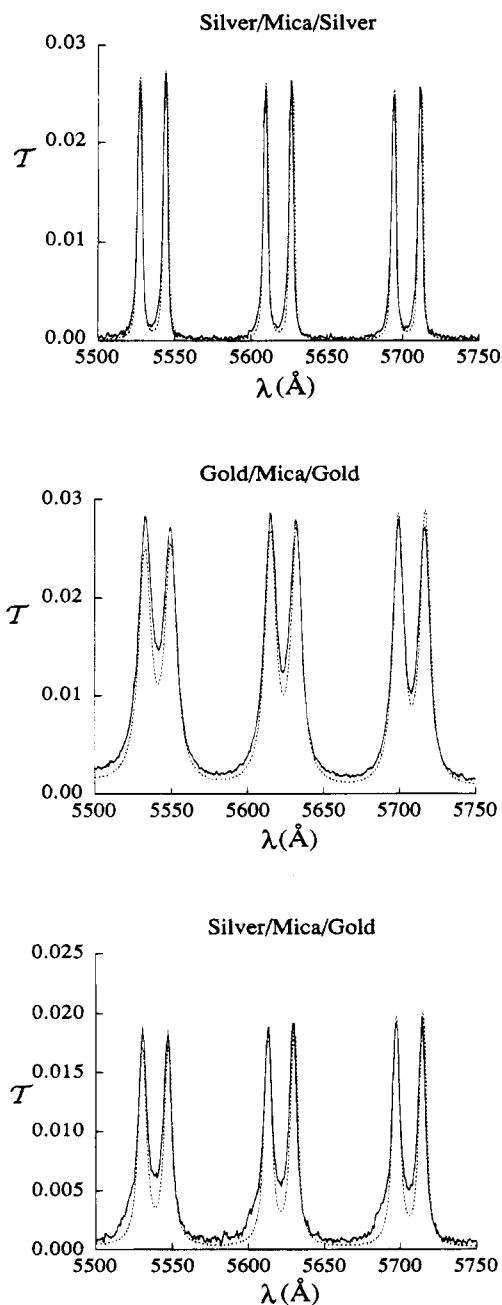


**Figure 6.** Measured and calculated  $\mathcal{T}$  for three filters. Each is composed of a single mica sheet, all of identical thickness, coated on both sides with 520 Å of metal. The first filter is coated with silver on both sides, the second is coated with gold on both sides, and the third with silver on one side and gold on the other. The determined mica thicknesses are 115 635 Å, 115 640 Å, and 115 645 Å, respectively.  $\bar{l}_0$  is 2529, 3444, and 2153, respectively.

described by Israelachvili.<sup>5</sup> They were coated on one side only by vacuum evaporation from a tungsten boat in a turbo-pumped Pyrex bell-jar system. Metals were 99.999% pure. Base pressure was better than  $8 \times 10^{-7}$  Torr during evaporation. Rates of evaporation were between 2.0 and 2.8 Å/s for gold and between 3.5 and 4.0 Å/s for silver. The

**Table 1.** Coefficients for Numerical Fit to Johnson and Christy's Data

	$a$	$b$ ( $10^{-3} \text{ \AA}^{-1}$ )	$c$ ( $10^{-7} \text{ \AA}^{-2}$ )
$n$ (silver)	0.05	0	0
$n$ (gold)	13.931	-4.3530	3.451
$k$ (silver)	-1.2300	0.87347	0
$k$ (gold)	-4.1877	1.2089	0

evaporation rate and the final film thickness were measured using a quartz crystal monitor. The coated mica sheets were then glued to cylindrical quartz support disks using the epoxy resin Epon 1004, with the metal side against the resin and the bare mica surface up. The supported mica sheets were then placed back in the evaporator and their bare surfaces were coated with metal, thus doubly-coating them. For the filter 2 experiment shown in Figure 5, however, the preparation was stopped after gluing the single-coated sheets to their supports.

The supported mica sheets were then mounted in our SFA<sup>16</sup> and white light from a tungsten-halogen lamp shone through them. The transmitted light was dispersed in a spectrometer. For the filter 2 experiment, two supported sheets were mounted with the bare mica surfaces opposed. The SFA was used to bring the mica surfaces into contact. Due to surface forces, the glue supporting the mica sheets deforms, creating a circular region of flat contact between the mica. The light transmitted through the flat region was used in the analysis.

## Appendix II: Refractive Indices

The exact values of refractive indices used for the theoretical calculations are described in this section. For ruby muscovite mica, the refractive indices measured by Israelachvili and Adams<sup>23</sup> were used.

$$\mu_{\text{mica}} = \mu_0 + \frac{4.76 \times 10^5 \text{ \AA}^2}{\lambda^2}$$

Because mica is birefringent, there are two values for  $\mu_0$ . They are  $\mu_0^\beta = 1.5795$  and  $\mu_0^\gamma = 1.5845$ .

The values of  $\mu^i$  and  $\mu^e$  used depended on how the supported interference filters were mounted in the SFA. For the doubly-coated mica either air or quartz (with resin) was on the incident side, with the other on the transmitted side. For air, we used  $\mu = 1.0$ ; for quartz/resin  $\mu = 1.5$ . For the filter 2 experiment (Figure 5), the quartz disks were on both the incident and transmitted sides.

Johnson and Christy<sup>22</sup> have measured  $n(\lambda)$  and  $k(\lambda)$  for gold and silver films at discrete wavelengths. We found these values fit well to linear functions over the wavelength range of interest (5200–6200 Å), except for  $n(\lambda)$  of gold, which is better described by a quadratic function. Shown in Table 1 are the coefficients of the fits to Johnson and Christy's data, where  $n$  and  $k$  are fit to the function,

$$f(\lambda) = a + b\lambda + c\lambda^2$$

and  $\lambda$  is in Å.

(23) Israelachvili, J. N.; Adams, G. E. *J. Chem. Soc., Faraday Trans. 1* 1978, 74, 975.